European Journal of Pharmaceutics and Biopharmaceutics 76 (2010) 357–365

Contents lists available at ScienceDirect

European Journal of Pharmaceutics and Biopharmaceutics

journal homepage: www.elsevier.com/locate/ejpb

Research paper

Differences between reversible (self-association) and irreversible aggregation of r*Hu*G-CSF in carbohydrate and polyol formulations

Renata Pavišić [a], Ivana Dodig [b], Anita Horvatić [b], Lucija Mijić [b], Mirela Sedić [b], Maša Rajić Linarić [c], Ita Gruić Sovulj [d], Tajana Preočanin [d], Mirjana Bukvić Krajačić [e], Mario Cindrić [b,*]

[a] *Hospira Zagreb, Zagreb, Croatia*
[b] *Department of Molecular Medicine, University of Zagreb, Zagreb, Croatia*
[c] *PLIVA Research and Development, Zagreb, Croatia*
[d] *Department of Chemistry, University of Zagreb, Zagreb, Croatia*
[e] *GlaxoSmithKline Research Centre, Zagreb, Croatia*

ARTICLE INFO

Article history:
Received 6 April 2010
Accepted in revised form 14 September 2010
Available online 18 September 2010

Keywords:
Aggregation
Self-association
r*Hu*G-CSF
Stabiliser
Asymmetric field-flow fractionation
Size-exclusion chromatography

ABSTRACT

Severe immunogenic and other debilitating human disorders potentially induced by protein aggregates have brought this phenomenon into the focus of biopharmaceutical science over the past decade. Depending on its driving forces, the process induced in the model protein r*Hu*G-CSF may be either reversible or irreversible, resulting in the assembly of self-associated protein species or irreversible aggregates of various final morphologies. The aim of our work was to investigate the correlation between irreversible and reversible aggregation and the protective effect of non-specific formulation stabilisers, selected from the group of carbohydrates and polyols including trehalose, xylitol, cellobiitol, turanose, cellobiose, leucrose, lactitol, lyxose, and sorbitol, against both irreversible protein aggregation and reversible self-association processes of the r*Hu*G-CSF. The formation of irreversible aggregates was thermally induced and evaluated using differential scanning calorimetry and size-exclusion chromatography. As opposed to the irreversible aggregation process, the process of self-association was induced by the agitation experiment by directly augmenting the protein solution contact surfaces. Absence of statistical connectivity between different stabilisers' ability to inhibit self-association or aggregation reactions indicates that these are two distinct physicochemical processes with different formulation stabilizing outcomes.

Reaction mechanism of thermally induced aggregation observed in the study was in line with published literature data, while the reaction mechanism for self-association process was postulated. The postulate has been verified experimentally by isothermal calorimetry and agitation set of experiments conducted after size-exclusion chromatography and asymmetrical flow field-flow fractionation separation of monomeric, dimeric, trimeric, oligomeric, and large self-associated forms detected on multi-angle light scattering, fluorescence, UV, and refractive index detectors. Besides defining the mechanism and kinetic of self-association in stabilized rHuG-CSF formulations, special attention was also paid to the shifts and ranks of the free energy of the aggregation or self-association transition states.

1. Introduction

The immunogenicity of protein aggregates and their ability to cause debilitating human disorders (e.g., Alzheimer's disease, Parkinson's disease, Huntington's disease, amyotrophic lateral sclerosis, and prion disease) by depositing in the body have made protein aggregation one of the most studied protein degradation processes in biopharmaceutical science in the past decade [1–4]. Therefore, prevention of protein aggregation is a prerequisite for successful production, storage, and administration of biopharmaceuticals. By practically employing the results of rationally developed aggregation studies in the process of selection of protein formulation stabilisers, researchers can successfully avoid the conditions that promote the formation of immunogenic impurities during products' life cycles [5–9].

Protein aggregation behaviour, such as onset, aggregation rate, and the final morphology of the aggregated state (i.e., amorphous precipitates or fibrils), has been found to depend strongly on the properties of a proteins solution environment, as well as on the relative intrinsic thermodynamic stability of its native state. Because aggregation can be induced by a wide variety of stressors, such as elevated temperature or agitation, it has been hypothesised that different stressors might favour different intermediate states,

* Corresponding author. Ruđer Bošković Institute, Department of Molecular Medicine, Bijenička cesta 54, 10000 Zagreb, Croatia. Tel.: +385 1 2356 676; fax: +385 1 2352 678.
E-mail address: mario.cindric@irb.hr (M. Cindrić).

0939-6411/$ - see front matter © 2010 Elsevier B.V. All rights reserved.
doi:10.1016/j.ejpb.2010.09.006

resulting in different secondary structures in the final aggregated state [7,10]. Depending on its driving force, the process may be reversible or irreversible resulting in the assembly of self-associated protein species or irreversible aggregates. Both irreversible aggregation and reversible self-association were induced in a set of experiments to investigate a possible correlation between these two processes and to evaluate the protective effect of potential recombinant human granulocyte colony stimulating factor (r*Hu*G-CSF) formulation stabilisers.

Widely administered r*Hu*G-CSF has been the focus of many aggregation studies [6,11,12], not only due to its physicochemical properties and sensitivity to aggregation but also due to its frequent and well-established therapeutic use for the treatment of neutropenia of various aetiologies and for the mobilisation of peripheral blood progenitor cells [13]. The r*Hu*G-CSF used as a model in the present research is a non-glycosylated, 175-amino-acid protein of 18.8 kDa produced in *Escherichia coli*. This cytokine macromolecule belongs to a distinct structural class of growth factors that contain a four-helical bundle (103 out of 175 aa) with a left-handed twist and overall dimensions of 45 Å × 26 Å × 26 Å. The structure of r*Hu*G-CSF is stabilised by two intramolecular disulfide bonds, both of which are required for activity. The molecule also contains one free cysteine residue responsible for an additional disulfide bond formation or exchange [14].

An extra disulfide bond formation or exchange can initiate what is probably the most common pathway of irreversible protein aggregation [5,15]. We thermally induced the formation of irreversible aggregates with an extra disulfide bond in the tested model protein formulations. Differential scanning calorimetry (DSC) was used to obtain information on the thermal stability of proteins under different solvent conditions. Scanning calorimetry was performed at different heating rates to obtain kinetic data on the aggregation process. The apparent activation energy of the thermally induced protein aggregation was estimated in this way [16–19]. Activation energies obtained on different protein/potential stabiliser formulations using DSC were further correlated with the size-exclusion chromatography (SEC) results obtained after both agitation experiments and sample incubation at elevated temperatures.

The mechanism of irreversible aggregation induced by thermal stress of r*Hu*G-CSF can be described by the following Lumry–Eyring equation framework [5,20]:

$$2N \leftrightarrow 2N^{*} \rightarrow A_2$$

$$N^{*} + A_n \rightarrow A_{n+1}$$

$$A_2 + A_m \rightarrow A_{m+2}$$

These equations describe a second-order reaction that depends on the formation of A_2 (a dimer). N is the native protein, and N^{*} represents the transition state; A_n is an aggregation-competent intermediate on the free Gibbs energy scale (*G vs.* reaction coordinate) one step away from the formation of A_m that represents aggregates (Fig. 1).

As opposed to the irreversible aggregation process, the less frequently studied process of self-association is induced by different physicochemical changes. Self-association is generally believed to be the result of hard-sphere, hydrophobic, electrostatic, van der Waals' and other similar short-range protein–protein interactions [21,22]. Compared to thermal denaturation experiments that induced formation of irreversible aggregates, agitation experiments that induced r*Hu*G-CSF self-association were correlated more with the protein solution contact surface (glass, plastic, and air), protein concentration, and volume of stressed solution. r*Hu*G-CSF is highly positively charged at the pH (4.0) of the tested formulations, meaning that strongly repulsive forces had to be overcome for the association process to occur. The self-association mechanism of reversible aggregation induced by agitation stress of r*Hu*G-CSF can be described by the following equations:

$$N \leftrightarrow N^{a*}$$

$$N^{a*} + A_{an} \leftrightarrow A_{an+1}$$

$$A_{an+1} + N^{a*} \leftrightarrow A_{an+2}$$

$$A_{an+2} + N^{a*} \cdots \leftrightarrow A_{am}$$

N is the native protein, and N^{a*} represents a transition state induced only by agitation; A_{an} is a self-association competent intermediate, and it successively increases to A_{am}, which represents the largest self-associated form of the protein (Fig. 1). These equations were experimentally supported by the isothermal calorimetry and agitation sets of experiments conducted after size-exclusion chromatography and asymmetrical flow field-flow fractionation (AF4)

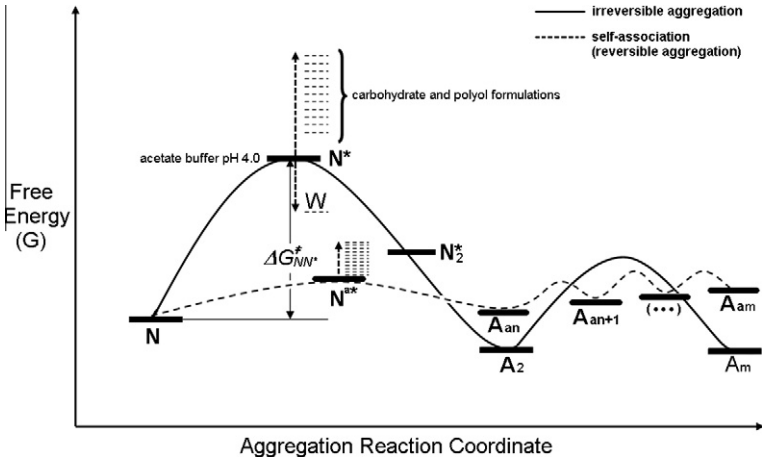

Fig. 1. Solid line indicates reaction coordinate diagram of r*Hu*G-CSF irreversible aggregation. N^{*} and N_2^{*} represent transition state species, and $\Delta G^{\ddagger}_{NN^{*}}$ activation free energy of aggregation. A_2 represents aggregation-competent intermediate, irreversible species responsible for reaction irreversibility and larger aggregates formation (A_m). Relative to the protein native state (N), doted arrows represent shifts in the free energy when carbohydrate or polyol stabilisers or tungsten (W) were added. Dotted line indicates reaction coordinate diagram of r*Hu*G-CSF reversible aggregation. N^{a*} represent transition state specie. A_{an+1}, A_{an+2}, and (•••) represent aggregation-competent intermediates responsible for larger self-associated form formation (A_{am}) and reaction reversibility. Dotted arrows next to N^{a*} represent shifts in the free energy when carbohydrate or polyol stabilisers were added (N^{a*} shifts are significantly smaller relative to N^{*} shifts).

separation of monomeric, dimeric, trimeric, oligomeric and large self-associated protein forms detected by multi-angle light scattering (MALS) and UV [23].

In general, this type of model can establish relationships between growth factors and cytokine self-association processes based on *in vitro* experiments and structural similarities/dissimilarities, and further on, connections between self-association (reversible aggregation) and irreversible aggregation in protein formulations. The central question of why some cytokines associate and disassociate so easily should have a mechanistic starting point and further physiological explanation that at the moment does not exist. Besides defining the mechanism and kinetics of self-association in tested protein formulations, special attention was paid to the shifts and ranks of the free energy of the aggregation or self-association transition states (N^* or N^{a*}, Fig. 1) where the following carbohydrates and polyols were added (pH 4.0): trehalose dihydrate, xylitol, cellobiitol, turanose, cellobiose, leucrose, lactitol monohydrate, lyxose, and sorbitol. To facilitate the interpretation of the results, we tested a non-formulated sample composed solely of protein in acetate buffer (pH 4.0) and a sample composed of protein in acetate buffer, (pH 4.0) stabilised by sorbitol, both prepared without the addition of polysorbate. The absence of surfactant in the control sample containing sorbitol resulted in the highest measured amount of dimer, aggregated, self-associated, oxidised and deamidated forms. Subtle differences between different carbohydrates and polyols could not be evaluated without polysorbate addition in the formulation.

Because reversible self-association has not been examined in many aggregation studies [24,25], we made an attempt to find the correlation between the two processes of reversible self-association and irreversible aggregation. Structurally different stabilisers can yield similar effects, as they act by being preferentially excluded from the surface of the protein, thus creating the thermodynamic conditions that would allow the protein to maintain its native conformation in spite of an adverse environment. The statistical connectivities between different stabilisers' abilities to inhibit self-association or aggregation reactions should be strongly correlated if connectivity between these two processes exists.

2. Materials and methods

2.1. Materials

Recombinant methionyl human granulocyte colony stimulating factor (r*Hu*G-CSF), expressed in *E. coli,* was produced by Hospira Zagreb (Zagreb, Croatia). The tested stabilisers D-(+)-trehalose dihydrate; xylitol, minimum 99%; and cellobiitol, minimum 98%, were purchased from Sigma Aldrich (St. Louis, USA). D-(+)-turanose, ~99%; D-(+)-cellobiose, ⩾99.0%; D-leucrose, ⩾98.0%; and D-lactitol monohydrate, Puriss grade, ⩾99.0% were purchased from Fluka (Buchs, Switzerland) and D-lyxose, 99% was purchased from Fluka (Milwaukee, Switzerland). Sorbitol, European Pharmacopoeia (Ph. Eur.) quality, was purchased from Roquette (Lestrem, France). Polysorbate 80, Ph. Eur. quality, was purchased from J.T. Baker (Phillipsburg, USA). Glacial acetic acid, Ph. Eur. quality, and sodium hydroxide, Ph. Eur. quality, were purchased from Merck (Darmstadt, Germany). Water for injections, produced by Hospira Zagreb (Zagreb, Croatia), was used for the preparation of formulations.

2.2. Preparation of protein formulations

r*Hu*G-CSF formulations were prepared by ultrafiltration of concentrated r*Hu*G-CSF solution (protein concentration 2.9 mg/ml in NaCl solution) into the placebo formulation. The ultrafiltration step was repeated three times at 5000 g using the Millipore Centrifugal Filter Device Centricon YM-10, 10,000 MW cut-off. Each placebo formulation contained a single potential stabiliser: D-(+)-trehalose dihydrate, xylitol, cellobiitol, D-(+)-turanose, D-(+)-cellobiose, D-leucrose, D-lactitol monohydrate, D-lyxose, or sorbitol at a concentration of 50 mg/ml and 10 mM sodium acetate buffer used to adjust the pH to 4.0 (the buffer was prepared by titration of acetic acid with sodium hydroxide solution). In the subsequent ultrafiltration step, polysorbate 80 was added to each of these nine prepared samples to achieve a final concentration of 0.04 mg/ml. The tested samples, when brought up to the starting volume using the placebo formulation, contained 2.9 mg/ml protein.

Two control samples without the addition of polysorbate 80 were prepared. The non-stabilised sample was prepared by ultrafiltration of concentrated r*Hu*G-CSF solution into 10 mM acetate buffer (pH 4.0) (serving as the placebo formulation for this sample), which was further used for dilution to the starting volume, resulting in a protein concentration of 2.9 mg/ml. The sample formulated with sorbitol only (referred to as "sorbitol without polysorbate" further in the text) was prepared in the same way as the non-stabilised sample, using the sorbitol placebo formulation for the ultrafiltration and final dilution steps.

2.3. Size-exclusion chromatography and asymmetric flow field-flow fractionation analysis of aggregates and self-associated forms by UV and MALS evaluation

2.3.1. Size-exclusion chromatography analysis

Dimers, oligomers, aggregates, and self-associated forms were separated by size-exclusion chromatography on an Agilent 1100 HPLC system from Agilent Technologies (Wilmington, Germany) using the TSKgelG3000SWXL 7.8 mm × 3000 mm and 5 μm particle size columns (Tosoh Bioscience, Stuttgart, Germany) and were detected by UV diode array detection at 215 nm (Bw 4 nm) with the reference wavelength set at 450 nm (Bw 80 nm). Detection was also performed on a MALS (multi-angle light scattering) detector (DAWN® HELEOS, Wyatt Technologies, CA, USA). The column temperature was maintained at 30 °C. The mobile phase consisted of 50 mM ammonium hydrogen carbonate (pH 7.0) at a flow rate of 0.5 ml/min. Samples were diluted to about 0.4 mg/ml using the placebo formulation solutions, and an aliquot of 20 μl was injected prior to analysis. The total time for chromatographic elution was 30 min. While in the autosampler tray, samples were maintained at 7 °C.

The self-association process was induced by the agitation of the protein formulation solution (0.4 mg/ml) in a 1.5-ml plastic tube using a mini shaker at 2600 rpm. The volume of each stressed solution was 100 μl, and the analysis was performed immediately after agitation for the following time periods: 10, 20, 30, 40, 50, 60, 70, 80, 90, 100, 110, 130, 160, 200, 250, and 300 s.

The molecular weights of aggregates and self-associated forms were calculated by collecting and evaluating the MALS and UV signals using the ASTRA Software from Wyatt Technology. The amounts of aggregates and self-associated forms were determined by collecting and evaluating their UV signals with the ChemStation Software from Agilent Technologies.

2.3.2. Asymmetric flow field-flow fractionation MALS analysis

The asymmetrical flow field-flow fractionation (AsFlFFF or AF4) channel was cut out of a 490-μm plastic spacer and positioned between a membrane and a glass wall in a Lucite Plexiglas block with a porous ceramic frit. The NADIR UF 10-C regenerated cellulose ultrafiltration membrane (Hoechst, Wiesbaden, Germany), with a molecular cut-off mass of 10,000, was used. A MALS instrument from Wyatt Technology and a UV–VIS diode array detector (DAD) from Agilent Technologies were connected on-line to the AsFlFFF

channel. Detection was performed on the MALS detector by monitoring light scattering at 90° and on the DAD at 215 nm (Bw 4 nm) with a reference wavelength of 450 nm (Bw 80 nm).

Ten microliters of undiluted sample was injected at an injection flow rate of 0.5 ml/min using a high performance liquid chromatography pump and injector. During the injection cycle and focusing, the inlet flow rate to the channel was 2.3 ml/min. An HPLC pump delivered the mobile phase to the channel in both directions, thus focusing (with a focus flow of 0.8 ml/min) the sample in a narrow band after the injection. After injection and focusing, the direction of the inlet flow was reversed from the inlet to the outlet, which enabled splitting of the applied flow into an axial flow through the channel (with a detector flow of 1 ml/min) and a perpendicular cross flow (with a gradient from 1 ml/min to 0 ml/min in 8 min). The carrier solution consisted of 50 mM ammonium hydrogen carbonate buffer (pH 7.0). The molecular weights of the aggregates and self-associated forms were calculated by collecting and evaluating the MALS and UV-DAD signals with the ASTRA Software from Wyatt Technology.

2.4. Thermal aggregation and denaturation by differential scanning calorimetry (DSC)

Thermally induced aggregation and denaturation were monitored using differential scanning calorimetry on a DSC Q100 (TA instruments, NJ, USA). The samples were measured in hermetically sealed platinum pans containing 30 µl of test solution. Prior to analysis, the samples were concentrated to 10 mg/ml r*Hu*G-CSF by ultrafiltration. The same amount of the corresponding placebo solution was used. Scanning calorimetry was performed at different heating rates (1–2.5 °C/min) in a temperature range of 35–90 °C. After the end of the first heating cycle, the protein sample was quickly cooled to 35 °C and rescanned again. The first scan was taken of the native protein, whereas the second scan was of heat-treated protein. The data were analysed using the TA Universal Analysis 2000 software. The isoconversional method was used to estimate the activation energy using the data obtained by DSC measurements. For a series of DSC measurements at heating rates β_{1-n}, and with $T_m j$ being the maximum of the endothermic peak j, the diagram $\log \beta_j = (1/T_{mj})$ is a line with the coefficient:

$$\frac{d(\log \beta)}{d(1/T)} = -0.4567 \frac{E_a}{R}$$

The apparent activation energy of the thermally denatured protein was estimated using a diagram $\log \beta$ *vs.* $f(1/T)$ [20,26,27].

2.5. The thermodynamics of disassociation by isothermal calorimetry

The thermodynamics of the dissociation of agitation-induced r*Hu*G-CSF self-associated forms was examined using isothermal calorimetry (CSC 4200, Calorimetry Sciences Corporations, UT, USA). The 1.3-ml sample of the r*Hu*G-CSF solution (0.94 mg/ml), formulated in a sorbitol/polysorbate aqueous solution, was thermostated at 17.5 °C, agitated (300 s), and then placed in a thermostated calorimetric cell (25.0 °C). The exchanged heat was obtained from the measured power required to maintain the system at a constant temperature (P). The initial temperature decrease (measured power) due to the temperature difference between the calorimetric cell and the protein solution was followed by a temperature jump (measured power) in the reaction cell. The high temperature increase indicates the slow and spontaneous exothermic reaction of the disassociation of agitation-induced r*Hu*G-CSF, self-associated forms. To estimate the heat of self-associated forms' disassociation, we subtracted the heat exchanged as a result of the temperature difference between the calorimetric cell and reaction suspension. The control experiment was performed under the same conditions as described for the protein solution.

3. Results and discussion

3.1. Characterisation of aggregates and self-associated forms by MALS analysis

Aggregation species and mechanisms can be characterised by MALS even when the measured approximate size and mass of macromolecules appear to be the same [28,29]. Other techniques used for the measurement of high molecular mass species, such as SEC-UV, SEC-FLD (calibration curve based on retention time) or analytical ultracentrifuge, can be explored as alternative orthogonal methods to SEC-UV/MALS. The size-exclusion calibration curve obtained by the retention time of protein calibrants was exponential and exhibited large experimental errors when measuring masses higher than 1×10^6 g/mol; therefore, it was not used for the accurate mass measurement of the molecular mass and size of aggregates.

This experiment was designed to distinguish between irreversible aggregates and large self-associated species. Samples already containing thermally induced aggregates (more than 2%, as measured by SEC-UV) produced by incubation at 40 °C for three months were further subjected to 2 min of agitation stress to produce self-associated species. SEC-UV/MALS chromatograms of the masses of the incubated r*Hu*G-CSF samples formulated with sorbitol/polysorbate (pH 4.0) were compared before and after the agitation step (Fig. 2A). Irreversible aggregates and large self-associated forms were co-eluted between 10 and 12 min. Except for the 20% increased peak area obtained for the additionally agitated sample, we could not define any notable changes by SEC-UV because the retention time remained the same. The separate analysis of large self-associated forms was hindered by the presence of a small

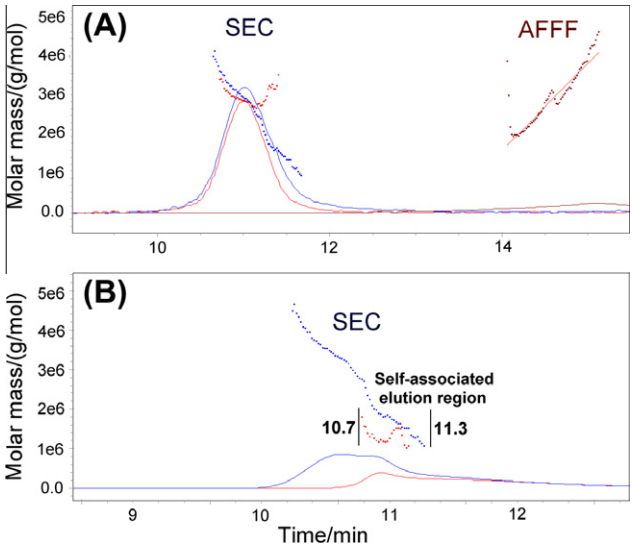

Fig. 2. Average MW of r*Hu*G-CSF (stabilized with sorbitol/polysorbate) irreversible aggregates and large self-associated forms measured by SEC-UV/MALS and AF4-UV/MALS (A) overlaid size-exclusion chromatograms obtained after thermal stress (red line), after thermal stress and agitation (blue line), and AF4 fractogram obtained after thermal stress (cherry-red line) and (B) size-exclusion chromatograms obtained after thermal stress and agitation (blue line) and agitation of sample without observed irreversible aggregates before agitation (red line). Note: While SEC elutes molecules with large hydrodynamic radius early in chromatogram, AF4 elutes the same molecules at the end of fractogram.

amount of irreversible aggregates that always remained attached to the column after consecutive SEC analyses of thermally stressed samples; these aggregates were eluted in subsequent runs.

The SEC-UV/MALS chromatograms of thermally stressed samples before and after 2 min of agitation were additionally overlaid with fractograms obtained by AF4-UV/MALS analysis of the sample that was only thermally stressed (the diffused peak of irreversible aggregates eluted after 14 min is depicted in Fig. 2A as a cherry-red line). The molecular weight (MW) distribution measured by SEC-MALS was homogeneous where the sample that was only thermally stressed was measured (the average MW = 3.3×10^6 g/mol, depicted in Fig. 2A as red dots). After agitation of the same sample, the MW distribution was more heterogeneous and ranged from 1.0×10^6 to 4.0×10^6 g/mol (the average MW = 2.7×10^6 g/mol; blue dots in Fig. 2A). The accurate agreement of the average MW data of the thermally stressed samples was observed for both analytical techniques used, SEC-MALS and AF4-MALS. Although AF4-MALS results were more diffused due to the broadening of the aggregates' peak, both experiments gave the same average MW for irreversible aggregates (3.3×10^6 g/mol; cherry-red dots in Fig. 2A). Consecutive measurements of the same sample and applied variations in SEC flow rate and aggregate concentration (±50%) did not affect the MW measurement significantly. This indicates that the observed broadening of the AF4 peak contributed to an experimental error in the range of $3.3–3.5 \times 10^6$ g/mol (the same experimental error was observed in SEC experiments). Unfortunately, size-exclusion chromatography cannot separate irreversible aggregates and large self-associated species efficiently, making the correlation between the measured retention time and the molecular weight unreliable.

In the second experiment, samples with and without thermally induced aggregates were subjected to agitation and subsequently analysed by SEC-UV/MALS. The overlaid chromatograms are shown in Fig. 2B (blue lines and dots and red lines and dots, respectively). The size-exclusion chromatography–MALS measurement of the MW of large self-associated forms (depicted by red dots in Fig. 2B) produced by samples without thermally induced aggregates exhibited an average MW of 1.3×10^6 g/mol with an experimental error of 15% with homogeneous MW distribution. Conversely, the same MW heterogeneity was observed in thermally stressed samples after agitation, as shown in Fig. 2A (blue dots). The measured MW plot explains the heterogeneous MW distribution caused by co-elution of self-associated forms and irreversible aggregates in the agitated, thermally stressed samples (blue dots in Fig. 2B).

The agreement between SEC- and AF4-MALS of average MW demonstrates the validity of the MW measurements, obtained by two different separation techniques, of the irreversible aggregates before and after agitation. The broad peak obtained by AF4 on agitated self-associated samples without irreversible aggregates contributed to a large experimental error in six repeated experiments (>35%); therefore, only the average MW measurement of the self-associated forms by AF4 was considered unreliable.

3.2. Kinetics of aggregation and self-association

The kinetics of the self-association process in the r*Hu*G-CSF formulations was analysed by SEC-UV chromatography (Fig. 3). The self-association process was induced by agitation of 100 µl of each sample, at a protein concentration of 0.4 mg/ml, using a shaker at 2600 rpm. The samples were agitated for 10, 20, 30, 40, 50, 60, 70, 80, 90, 100, 110, 130, 160, 200, 250, or 300 s and immediately analysed. As opposed to the experimental conditions of agitation with fast kinetics of the self-associated forms, the thermally induced aggregation experiment was extremely demanding and sometimes unfeasible to conduct. It required long experimental times and quantitative analysis of only two aggregate species, a dimer that was slightly above 0.1% of the total area and aggregates that were first detected only after one week of thermally stressing the sample at 40 °C. The chromatogram of thermally induced aggregates is shown in Fig. 4. The tungsten experiment involved a two-month-long incubation at 2.5 ppm, culminating in the acceleration of the formation of aggregates at room temperature, thus making the experiment inappropriate for kinetic experiments. The conditions of the SEC experiment made it the most applicable for this kinetic study.

Interestingly, the mechanism of association seemed to be highly dependent on the protein environment, as substantially different time courses were observed for the formulated protein solutions that were tested (Fig. 3). The complexity and diversity of the chromatographic curves (Fig. 5) probably reflect the intricacy of the self-association process under the given conditions. From the results of our real-time analysis, we conclude that the formation of dimers is generally greater than the formation of oligomers or aggregates. Only in the presence of sorbitol and leucrose did aggregates accumulate to the same or higher concentration than dimers.

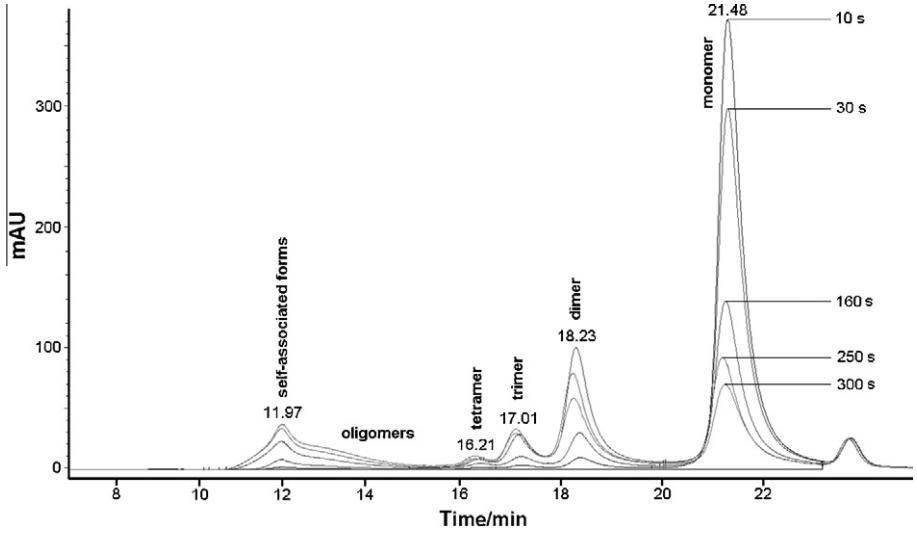

Fig. 3. Size-exclusion chromatograms of r*Hu*G-CSF sorbitol/polysorbate stabilizing solution agitated for 10, 30, 160, 250, and 300 s (protein concentration of 0.4 mg/ml, 1.5 ml plastic tube, volume of 100 µl of stabilizing protein solution).

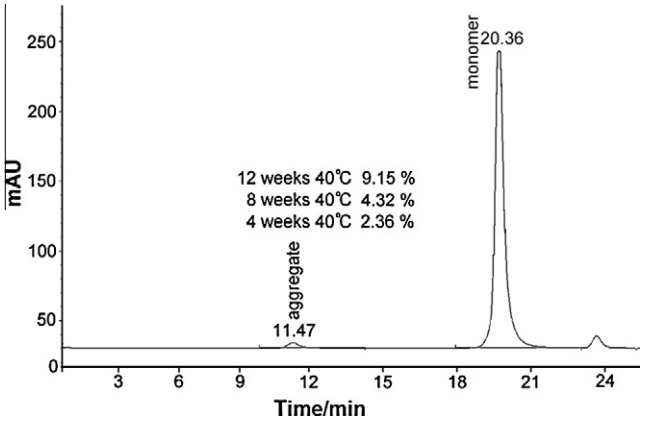

Fig. 4. Size-exclusion chromatogram of r*Hu*G-CSF sorbitol/polysorbate stabilizing solution after 4 weeks of thermal stress at 40 °C (protein concentration of 0.4 mg/ml).

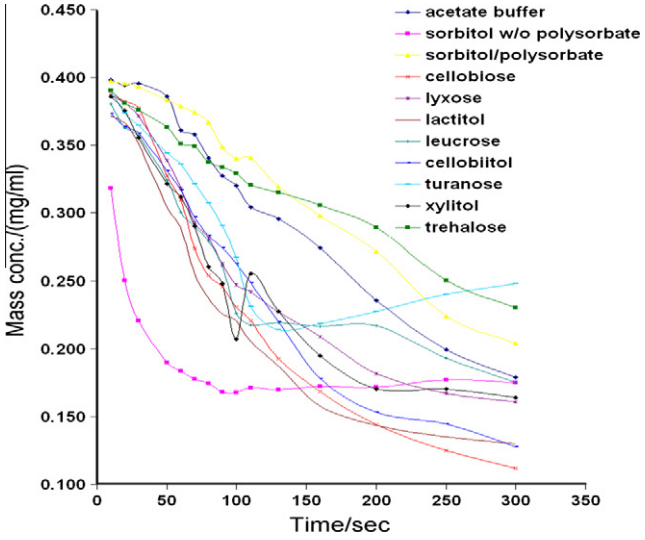

Fig. 5. r*Hu*G-CSF monomer evanescence in the presence of different stabilisers as a function of agitation time.

Thus, it seems that the aggregation of r*Hu*G-CSF may occur through the fast formation of dimers followed by slow, additional aggregation.

When we compared monomer evanescence in different protein formulation environments, it was clear that agitation for 300 s in the presence of cellobiose, lactitol and cellobiitol led to the distinctive monomer self-association cascade reactions (Fig. 5). The presence of lyxose and leucrose suppressed the formation of self-associated forms in comparison with the control samples, sorbitol without polysorbate and the non-stabilised sample (acetate buffer). When agitation was performed in the presence of sorbitol with the addition of polysorbate, the formation of dimers and self-associated forms was substantially diminished. However, in the absence of polysorbate, a faster formation of dimers (and oligomers) was observed as expected, given the important role of this compound in the prevention of agitation stress of r*Hu*G-CSF (Figs. 5 and 6).

The formation of self-associated forms was largely suppressed in the presence of turanose, sorbitol with the addition of polysorbate, and trehalose, making those stabilisers promising stabilising agents. Turanose was the only stabiliser that extended the plateau after 110 s, whereas the other stabilisers continued to associate even after 300 s (except sorbitol without polysorbate at a low plateau level). However, dimer formation was still substantial under this condition.

3.3. Thermal aggregation and denaturation by differential scanning calorimetry, compared to size-exclusion chromatography of reversible and irreversible aggregations

Differential scanning calorimetry is an excellent tool for the determination of heat absorption at elevated temperatures, as the technique directly measures the forces stabilising the native conformation of a protein and the effect on these forces of additives in solution. A non-isothermal method used for the determination of kinetic parameters is advantageous for the rapid collection of data. For each of the formulations tested, the scans were taken at a range of temperatures from 35 °C to 90 °C. The scans of the native protein exhibited an endothermic transition. The sample was then quickly cooled to 35 °C and rescanned. The scan of the heat-treated protein exhibited no thermal transition, indicating that the protein was irreversibly denatured during the heating process. The heating rate was between 1.0 °C/min and 2.5 °C/min. The results show a heating rate dependency evidenced by the increase in the thermal unfolding temperature with an increase in the heating rate, indicating that the thermal denaturation of r*Hu*G-CSF is kinetically controlled [30].

A DSC scan of the r*Hu*G-CSF sample formulated with turanose and taken at a heating rate of 2.5 °C/min is presented in Fig. 7. The isoconversional method was used to estimate the activation energy of the aggregation process. Using the data from DSC conversion plots, according to the equation given in Section 2.4, the apparent activation energy of the thermally induced aggregation of the protein was estimated from the isoconversional plot of log β *vs.* $1/T$. This rapid screening method was used primarily to compare the response patterns of different potential stabilisers when assessing their effectiveness against thermal aggregation. The calculated values of the activation energies ranged from 162.2 kJ/mol for the stabiliser lyxose to 490.3 kJ/mol for the sample formulated with sorbitol but no polysorbate. Table 1 shows that the activation energies of the aggregation process obtained by the DSC experiment were correlated with the reaction rate constants obtained using the SEC-UV data of thermally induced aggregates analysis (35 days of temperature stress at 40 °C) and with reaction rate constants of the self-association process (an agitation experiment for 10–300 s and the SEC-UV data). The Pearson correlation at a confidence level of 95% was performed using the SPSS 16.01 for Windows software (SPSS Inc., Chicago, Illinois).

There was low correlation between the DSC irreversible aggregation experiment and the SEC-UV reversible aggregation reaction rate constants ($R = -0.245$; $P > 0.05085$); therefore, the activation energy levels of N^* and N^{a*} cannot be compared. Overall, the driving forces of irreversible and reversible aggregation are not connected; therefore, the formulation additives that prevent one process probably will not prevent the other. This result was not entirely unexpected because the mechanisms of protein, carbohydrate, or polyol stabilisation should theoretically prevent either irreversible or reversible aggregation (stabilisers are preferentially excluded from the surface of the protein in both cases; protein collisions and protein–protein contact should therefore be minimised).

Similarly, the correlation between the reaction rate constants of the irreversible and reversible aggregation of r*Hu*G-CSF obtained by the SEC-UV method was low (0.350, $P < 0.05$), with a level of 0.6 denoting strong statistical significance.

In contrast, statistical significance ($R = -0.808$; $P < 0.05$) was achieved when the DSC irreversible aggregation data were

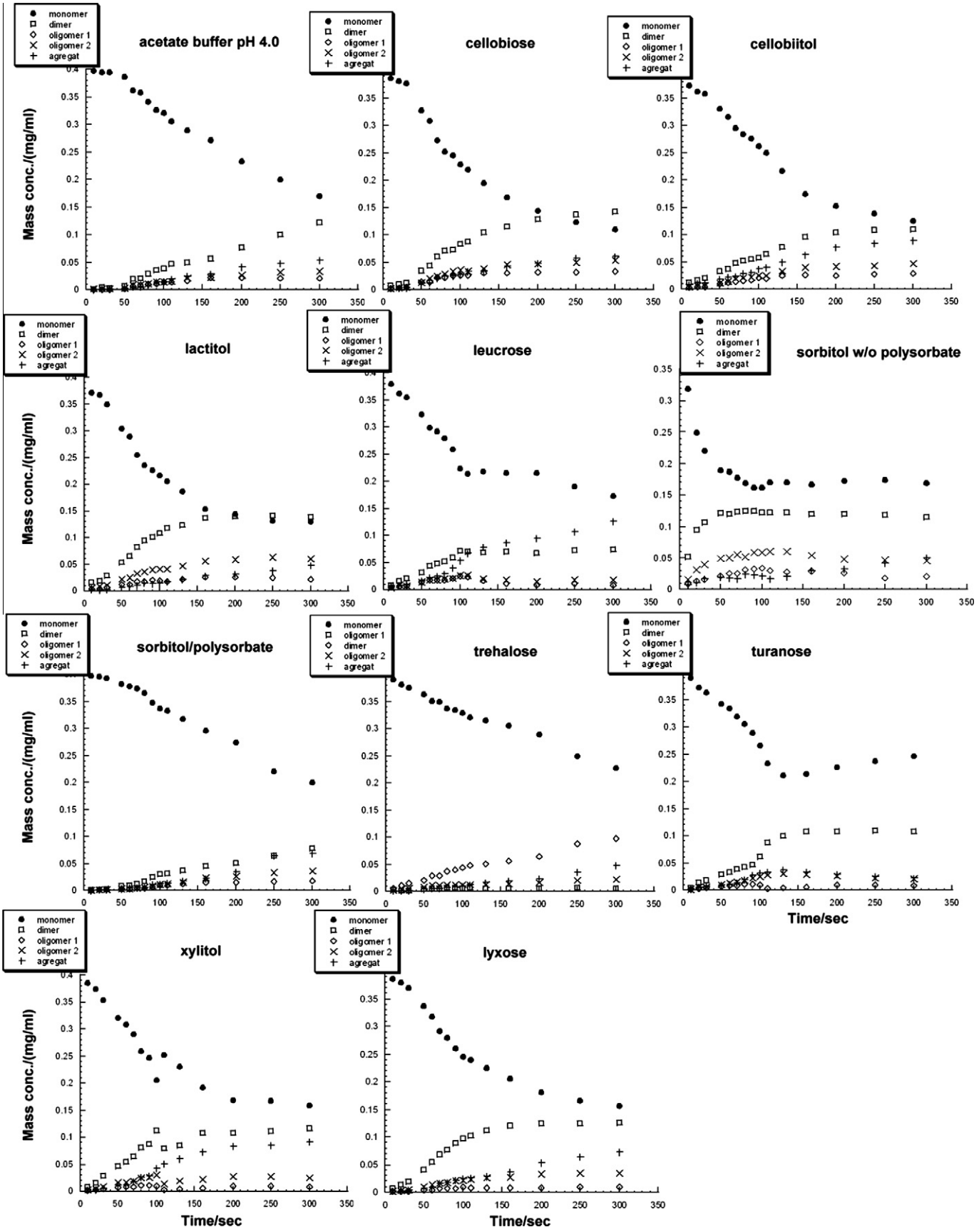

Fig. 6. r*Hu*G-CSF monomer evanescence, dimer, trimer, tetramer, and self-associated forms development in the presence of different stabilisers as a function of agitation time.

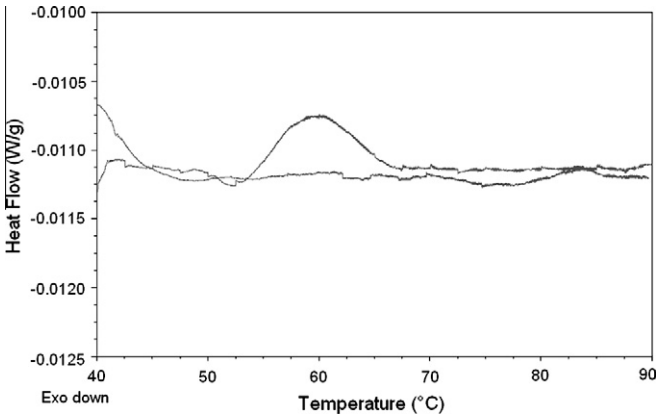

Fig. 7. DSC curves for the influence of stabiliser turanose on the thermal denaturation of r*Hu*G-CSF 10 mg/ml, at a 2.5 °C/min heating rate.

Table 1
Calculated activation energy for the aggregation process of r*Hu*G-CSF in different protein formulations, calculated reaction rate constants of irreversible aggregation formation during 35 days of temperature stress at 40 °C, and aggregation reaction rate constants of agitation experiment (10–300 s) correlation.

Stabiliser	*Ea* (kJ/mol)	Irreversible aggregation ($10^5 \times k_1$ day^{-1})	Reversible aggregation (k_1 min^{-1})
D-lyxose	162.6	3.60	3.05
Turanose	164.0	1.52	3.32
Lactitol	168.6	3.17	2.06
Cellobiose	171.4	2.07	2.96
D-trehalose	173.1	3.64	1.62
Acetate buffer	318.6	1.63	2.13
Cellobiitol	363.5	1.53	4.64
Leucrose	379.3	1.39	6.35
Xylitol	403.4	1.10	4.73
Sorbitol	462.6	1.03	1.40
Sorbitol, no polysorbate	490.3	0.75	2.74
Correlation	*Ea*	Irreversible aggregation	Reversible aggregation
Ea	1		
Irreversible aggregation	−0.808[a] (0.0026)[b]	1	
Reversible aggregation	0.245 (0.57)[b]	−0.350 (0.29)[b]	1

[a] Correlation coefficient.
[b] *P* value.

correlated with the SEC-UV irreversible aggregation reaction rate constants for r*Hu*G-CSF. This correlation was expected and verified the validity of the correlation experiments (DSC irreversible aggregation *vs*. SEC-UV irreversible aggregation). Higher temperatures in the DSC experiment (the melting points of some of the tested carbohydrates were in the same temperature range as the scans) than in the SEC-UV experiment (one month at 40 °C) did not affect their performance as evidenced by a good correlation between these two sets of data.

3.4. The thermodynamics of the dissociation of self-associated forms as measured by isothermal calorimetry

Agitation of a protein solution can initiate protein collisions with different contact surfaces (e.g., glass, plastic or air), providing sufficient energy for the reversible formation of self-associated forms. After a short relaxation time of two hours, the largest self-associated form (A_{am}) successively and spontaneously disassociated to the monomeric form (N) by a dissociation reaction cascade described by the following equations:

$$A_{am} \rightarrow A_{an+2} + N^{a*}$$
$$A_{an+2} \rightarrow A_{an+1} + N^{a*} ldots$$
$$A_{an} \rightarrow N^{a*} \leftrightarrow N$$

The energy associated with the above-described dissociation process is the opposite of that involved in the formation of self-associated forms (described in Fig. 1). From the isothermal calorimetric measurements, the total reaction (the sum of all the steps in the dissociation process, shown in Fig. 8) is exothermic; $\Delta H \approx -23$ kJ per 1 mol monomers (r*Hu*G-CSF). A reversible association process induced by the agitation of r*Hu*G-CSF is described in Fig. 9. The dissociation process of self-associated forms occurred after the agitation of samples that initially contained irreversible aggregates (was confirmed by SEC-UV) (Fig. 2), but the quantity of self-associated forms decreased fivefold in comparison with the agitation of samples without irreversible aggregates. The decrease in self-associated forms was evidenced by a notable decrease in the quantity of large self-associated forms detected by SEC-UV and MALS. Consequently, the dissociation process could not be monitored by isothermal calorimetry due to a low yield of formation of reversible aggregates, although a 20% increase in the peak area of irreversible aggregates was detected, as described in Section 3.1. The free energies of the self-associated forms (A_{am}, A_{an+2}, A_{an+1}, A_{an}, ...) and monomers (N) are displayed on the arbitrary free energy *y*-axis, whereas the *x*-axis represents the course of individual reaction events.

After studying the thermodynamic profiles of the association and dissociation processes, we performed kinetic studies, and after a comparison of the effects on these processes caused by different protein formulations, it was postulated that the dissociation process consists of a series of energetically favourable exothermic reactions and that the increasing number of particles in the solution increases the entropy of the system, leading to the thermodynamically stabile monomer.

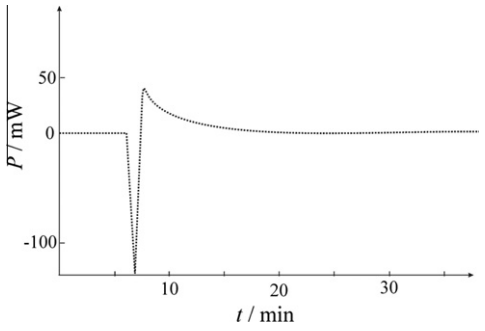

Fig. 8. Thermogram of exothermic dissociation of agitation-induced r*Hu*G-CSF self-associated forms.

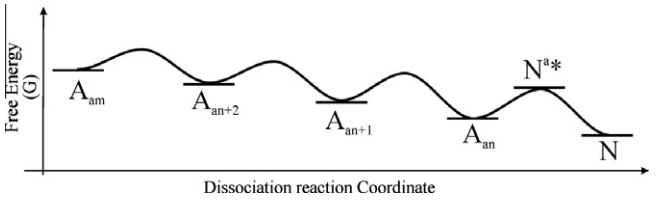

Fig. 9. Schematic reaction coordinate diagram of r*Hu*G-CSF of dissociation of self-associated forms on an arbitrary free energy *y*-axis. Curved lines illustrate kinetic energy barriers.

4. Conclusions

A robust and reliable multi-angle light-scattering-based method for differentiation and structural characterisation of mixtures of irreversible/reversible aggregates is presented here. Self-associated forms and irreversible aggregates have substantially different physicochemical properties, as established by the MALS method (size and molecular weight). The average molecular weight, A_{am}, measured by MALS of self-associated forms, ranged from 1.3×10^6 to 1.5×10^6 g/mol (with a hydrodynamic diameter of 40.8–42.8 nm). For irreversible aggregate forms, A_m ranged from 3.3×10^6 to 3.5×10^6 g/mol (with a hydrodynamic diameter of 53.2–55.4 nm). Size, as per measured molecular mass, indicated a possible dendritic shape of self-associated forms relative to the more common, compact shape assumed in the case of disulfide-bonded irreversible aggregates. Two separation techniques, asymmetric flow field-flow fractionation and size-exclusion chromatography, coupled with MALS, clearly defined the differences between aggregates and self-associated forms.

Irreversible and reversible aggregations are two dissimilar physicochemical processes with different thermodynamic, kinetic, and formulation-stabilising outcomes. Stabilisers that prevented irreversible aggregation could not prevent reversible aggregation and *vice versa* (the DSC *vs*. SEC-UV stabilisers correlation). The only possibility of convergence between r*Hu*G-CSF and N^* and N^{a*} (the transition state species of irreversible and reversible aggregation) would be a decrease in the N^* activation free energy of aggregation ($\Delta G^{\ddagger}_{NN*}$ decreased by pH, tungsten addition, etc.). In that case, irreversible aggregation might be induced by agitation. Some proteins with a large number of disulfide bonds (e.g., immunoglobulins) might be more susceptible to agitation-induced irreversible aggregation than would small cytokines due to the number and proximity of disulfide bonds [31]. In protein solutions where self-association is observed, a prolonged agitation force (2 days), plastic vessels with a large contact area, high protein concentrations, and formulations without the addition of polysorbate should be avoided.

Its ease of self-association and irreversible aggregation makes r*Hu*G-CSF a nearly ideal protein model for carbohydrate and polyol formulation testing. However, tests performed on only one model protein under laboratory conditions can be helpful (e.g., for thermodynamics, kinetics, and size/mass examination), but they cannot answer these unresolved questions: why do cytokines and some other classes of proteins generally make self-associated forms so easily, and does the reversible aggregation up to the size of almost 1.5×10^6 g/mol play an important role in the physiological processes of the organism? Nevertheless, a detailed physicochemical description of the phenomenon is a desirable starting point.

Acknowledgement

The authors would like to acknowledge the significant contribution made by Ana Kwokal.

References

[1] C.A. Ross, M.A. Poirier, Protein aggregation and neurodegenerative disease, Nat. Med. 10 (2004) S10–S17.
[2] M.E. Cromwell, E. Hilario, F. Jacobson, Protein aggregation and bioprocessing, AAPS J. 8 (2006) E572–E579.
[3] T. Ratovitski, M. Gucek, H. Jiang, E. Chighladze, E. Waldron, J. D'Ambola, Z. Hou, Y. Liang, M.A. Poirier, R.R. Hirschhorn, R. Graham, M.R. Hayden, R.N. Cole, C.A. Ross, Mutant huntingtin N-terminal fragments of specific size mediate aggregation and toxicity in neuronal cells, J. Biol. Chem. 284 (2009) 10855–10867.
[4] S.Y. Patro, T.M. Przybycien, Simulations of reversible protein aggregate and crystal structure, Biophys. J. 70 (1996) 2888–2902.
[5] E.Y. Chi, S. Krishnan, T.W. Randolph, J.F. Carpenter, Physical stability of proteins in aqueous solution: mechanism and driving forces in nonnative protein aggregation, Pharm. Res. 20 (2003) 1325–1336.
[6] R. Pavišić, K. Hock, I. Mijić, A. Horvatić, M. Gecan, M. Sedić, M.B. Krajačić, M. Cindrić, Recombinant human granulocyte colony stimulating factor pre-screening and screening of stabilizing carbohydrates and polyols, Int. J. Pharm. 387 (2010) 110–119.
[7] M.K. Goyal, I. Roy, U.C. Banerjee, V.K. Sharma, A.K. Bansal, Role of benzyl alcohol in the prevention of heat-induced aggregation and inactivation of hen egg white lysozyme, Eur. J. Pharm. Biopharm. 71 (2009) 367–376.
[8] F. He, S. Hogan, R.F. Latypov, L.O. Narhi, V.I. Razinkov, High throughput thermostability screening of monoclonal antibody formulations, J. Pharm. Sci. 99 (2010) 1707–1720.
[9] B.S. Chang, S. Hershenson, Practical approaches to protein formulation development, Pharm. Biotechnol. 13 (2002) 1–25.
[10] X. Wang, T.K. Das, S.K. Singh, S. Kumar, Potential aggregation prone regions in biotherapeutics: a survey of commercial monoclonal antibodies, MAbs 1 (2009) 254–267.
[11] J.T. Ribarska, S.T. Jolevska, A.P. Panovska, A. Dimitrovska, Studying the formation of aggregates in recombinant human granulocyte-colony stimulating factor (rHuG-CSF), lenograstim, using size-exclusion chromatography and SDS–PAGE, Acta Pharm. 58 (2008) 199–206.
[12] A.C. Herman, T.C. Boone, H.S. Lu, Characterization, formulation, and stability of Neupogen® (Filgrastim) a recombinant human granulocyte colony stimulating factor, in: R. Pearlman, Y.J. Wang (Eds.), Formulation, Characterisation and Stability of Protein Drugs, Plenum Press, New York, 1996, pp. 303–328.
[13] R. Thirumangalathu, S. Krishnan, D.N. Brems, T.W. Randolph, J.F. Carpenter, Effects of pH, temperature, and sucrose on benzyl alcohol-induced aggregation of recombinant human granulocyte colony stimulating factor, J. Pharm. Sci. 95 (2006) 1480–1497.
[14] C.P. Hill, T.D. Osslund, D. Eisenberg, The structure of granulocyte-colony-stimulating factor and its relationship to other growth factors, Proc. Natl. Acad. Sci. USA. 90 (1993) 5167–5171.
[15] W. Wang, Protein aggregation and its inhibition in biopharmaceutics, Int. J. Pharm. 289 (2005) 1–30.
[16] A.W. Vermeer, W. Norde, The thermal stability of immunoglobulin: unfolding and aggregation of a multi-domain protein, Biophys. J. 78 (2000) 394–404.
[17] T. Chen, D.M. Oakley, Thermal analysis of proteins of pharmaceutical interest, Thermochim. Acta 248 (1995) 229–244.
[18] B.S. Kendrick, J.L. Cleland, X. Lam, T. Nguyen, T.W. Randolph, M.C. Manning, J.F. Carpenter, Aggregation of recombinant human interferon gamma: kinetics and structural transitions, J. Pharm. Sci. 87 (1998) 1069–1076.
[19] X.-M. Cao, X. Yang, J.-Y. Shi, Y.-W. Liu, C.-X. Wang, The effect of glucose on bovine serum albumin denatured aggregation kinetics at high concentration: the master plots method study by DSC, J. Therm. Anal. Calorim. 93 (2008) 451–458.
[20] J.M. Sanchez-Ruiz, Theoretical analysis of Lumry–Eyring models in differential scanning calorimetry, Biophys. J. 61 (1992) 921–935.
[21] M. Gottschalk, K. Venu, B. Halle, Protein self-association in solution: the bovine pancreatic trypsin inhibitor decamer, Biophys. J. 84 (2003) 3941–3958.
[22] P.R. Wills, D.J. Winzor, Direct allowance for the effects of thermodynamic nonideality in the quantitative characterization of protein self-association by osmometry, Biophys. Chem. 145 (2009) 64–71.
[23] P. Gagnon, T. Arakawa, Aggregation detection and removal biopharmaceutical proteins, Curr. Pharm. Biotechnol. 10 (2009). 347–347.
[24] J.P. Gabrielson, K.K. Arthur, M.R. Stoner, B.C. Winn, B.S. Kendrick, V. Razinkov, J. Svitel, Y. Jiang, P.J. Voelker, C.A. Fernandes, R. Ridgeway, Precision of protein aggregation measurements by sedimentation velocity analytical ultracentrifugation in biopharmaceutical applications, Anal. Biochem. 396 (2010) 231–241.
[25] J. Liu, J.D. Andya, S.J. Shire, A critical review of analytical ultracentrifugation and field flow fractionation methods for measuring protein aggregation, AAPS J. 8 (2006) E580–E589.
[26] J.M. Sanchez-Ruiz, J.L. Lopez-Lacomba, M. Cortijo, P.L. Mateo, Differential scanning calorimetry of the irreversible thermal denaturation of thermolysin, Biochemistry 27 (1988) 1648–1652.
[27] T. Arakawa, J.S. Philo, D. Ejima, K. Tsumoto, F. Arisaka, Aggregation analysis of therapeutic proteins, Part 1: general aspects and techniques for assessment, BioProcess Int. 4 (2006) 42–43.
[28] D.R. Arifin, A.F. Palmer, Determination of size distribution and encapsulation efficiency of liposome-encapsulated hemoglobin blood substitutes using asymmetric flow field-flow fractionation coupled with multi-angle static light scattering, Biotechnol. Prog. 19 (2003) 1798–1811.
[29] Y. Li, B.A. Ogunnaike, C.J. Roberts, Multi-variate approach to global protein aggregation behavior and kinetics: effects of pH NaCl and temperature for alpha-chymotrypsinogen A, J. Pharm. Sci. 99 (2010) 645–662.
[30] H.J. Hinz, F.P. Schwarz, Measurement and analysis of results obtained on biological substances with differential scanning calorimetry, Pure Appl. Chem. 73 (2001) 745–759.
[31] M. Jimenez, G. Rivas, A.P. Minton, Quantitative characterization of weak self-association in concentrated solutions of immunoglobulin G via the measurement of sedimentation equilibrium and osmotic pressure, Biochemistry 46 (2007) 8373–8378.